MATERIALS CHEMISTRY FRONTIERS

RESEARCH ARTICLE

View Article Online
View Journal | View Issue

Cite this: *Mater. Chem. Front.*, 2020, **4**, 2018

The design of an extended multiple resonance TADF emitter based on a polycyclic amine/carbonyl system†‡

Dianming Sun,[ab] Subeesh Madayanad Suresh,[b] David Hall,[bc] Ming Zhang,[a] Changfeng Si,[b] David B. Cordes,[b] Alexandra M. Z. Slawin,[b] Yoann Olivier,*[cd] Xiaohong Zhang*[a] and Eli Zysman-Colman*[b]

Received 28th March 2020,
Accepted 13th May 2020

DOI: 10.1039/d0qm00190b

rsc.li/frontiers-materials

The development of multiple resonance thermally activated delayed fluorescence (MR-TADF) materials possessing narrow emission spectra has attracted significant attention as emitters for high colour purity organic light emitting diodes (OLEDs). In this work, a simple design strategy is introduced to construct an MR-TADF emitter, **DDiKTa**, through dimerization of the known MR-TADF emitter **DiKTa**. This design permits concentration quenching to be largely suppressed, which is a known weakness of previously reported MR-TADF emitters. OLEDs based on **DDiKTa** show an EQE_{max} of 19% at a doping concentration of 9 wt%. The electroluminescence spectrum is red-shifted into the green, producing a rare example of a green-emitting MR-TADF OLED.

1. Introduction

Thermally activated delayed fluorescence (TADF) emitters have attracted significant attention[1–5] as replacement candidates for phosphorescent organometallic complexes in organic light emitting diodes (OLEDs). Such materials are capable of recruiting 100% of the generated excitons for light production without the requirement of the heavy metal center to mediate intersystem crossing events between the excited singlet and triplet states. The most common strategy to achieve efficient TADF emitters is based on a twisted donor–acceptor molecular design[6] that promotes a reduction in the exchange integral between the highest occupied molecular orbital (HOMO) and lowest unoccupied molecular orbital (LUMO) due to localization of the electron density on the donor and acceptor moieties, respectively. Thus, a small energy gap between the lowest triplet and singlet excited states (ΔE_{ST}) is achieved that then permits the thermal up-conversion of triplet excitons to singlet excitons through reverse intersystem crossing (RISC).

However, with few exceptions,[7–11] the emission from TADF compounds is broad (typically, 0.45–0.55 eV; 80–110 nm), due to the charge-transfer (CT) character of the emission singlet state.[12] This leads to poor colour purity in the OLED. With the increasing commercial requirements for high-resolution OLED displays, new red, green and blue emitters need to be developed that show both potential for 100% internal quantum efficiency and narrow emission spectra, obviating the use of color filters and their associated energy loss.[13]

Recently, a new approach to TADF emitter design was reported by Hatakeyama *et al.* based on p- and n-doped nanographene compounds. The first example was the rigid boron–oxygen polycyclic aromatic framework, DOBNA (see Fig. S1 for structures of literature emitters, ESI†).[14] The presence of *para*-disposed boron and oxygen atoms in the compound possessing complementary resonance effects led to significantly separated electron densities between the HOMO and LUMO and a correspondingly small ΔE_{ST} of 0.15 eV. The emission of DOBNA unfortunately, is in the UV region, which was deemed too high in energy for this compound to be used as an emitter for OLEDs. The same group then reported the nitrogen-containing blue-emitting **DABNA-1**, which served as the first multiple resonance TADF (MR-TADF) emitter used in an OLED.[15] OLEDs employing **DABNA-1** exhibited an emission at λ_{EL} of 459 nm with an FWHM of 28 nm and the corresponding CIE coordinates of (0.13, 0.09), and with a maximum external quantum efficiency, EQE_{max}, of 13.5%. Further improvement in the

[a] *Institute of Functional Nano & Soft Materials (FUNSOM) and Jiangsu Key Laboratory for Carbon-Based Functional Materials & Devices, Soochow University, Suzhou, Jiangsu 215123, P. R. China. E-mail: xiaohong_zhang@suda.edu.cn*
[b] *Organic Semiconductor Centre, EaStCHEM School of Chemistry, University of St Andrews, St Andrews KY16 9ST, UK. E-mail: eli.zysman-colman@st-andrews.ac.uk*
[c] *Laboratory for Chemistry of Novel Materials, University of Mons, 7000, Mons, Belgium*
[d] *Unité de Chimie Physique Théorique et Structurale & Laboratoire de Physique du Solide, Namur Institute of Structured Matter, Université de Namur, Rue de Bruxelles, 61, 5000 Namur, Belgium*

† Electronic supplementary information (ESI) available. CCDC 1992507. For ESI and crystallographic data in CIF or other electronic format see DOI: 10.1039/d0qm00190b
‡ The research data supporting this publication can be accessed at https://doi.org/10.17630/1bec3f8b-84ae-4a1c-87da-9d36465f811b.

design was evidenced in **DABNA-2**, a suitably substituted analogue of **DABNA-1**, which produced a blue OLED with λ_{EL} of 467 nm, an FWHM of 28 nm and CIE coordinates of (0.12, 0.13), but with a much-improved EQE_{max} of 20.2%. Inspired by these early achievements, several derivatives have been reported. With the addition of *t*-butyl groups on the **DABNA-1** core, ***t*-DABNA** shows a shorter delayed lifetime and a consequently improved OLED efficiency roll-off.[16] By introducing carbazole, **TBN-TPA** exhibited a significantly improved performance with an EQE_{max} of 32.1% for a blue OLED.[17] The extended polycyclic framework of ***ν*-DABNA** results in a state-of-the-art deep blue OLED exhibiting an EQE_{max} of 34.4%.[18] Boranes are not the only acceptor motif used in MR-TADF emitters. Recently, ketone-containing MR-TADF emitters have been shown to produce blue to sky-blue OLEDs.[19,20] We showed that by decorating a MR-TADF emitter, **DiKTa**, with mesityl groups, **Mes$_3$DiKTa**, undesired aggregation caused quenching and excimer emission can be largely mitigated.[21]

Herein, we report the emitter **DDiKTa**, which is a dimeric compound consisting of two MR-TADF **DiKTa** units (Scheme 1). The slightly increased conjugation present in **DDikTa** compared to **DiKTa** contributes to a modest red-shifting of the emission; however, the new compound conserves its MR-TADF status. OLEDs employing **DDiKTa** showed blue-green emission with λ_{EL} of 500 nm and CIE coordinates of (0.18, 0.53) and a high EQE_{max} of 19% at a doping concentration of 9 wt% in DPEPO; at a doping concentration of 12 wt%, the EQE_{max} was 18.5%. To the best of our knowledge, there exists only a single report of green MR-TADF OLEDs with λ_{EL} ranging from 493–501 nm and EQE_{max} ranging from 21–22%.[22] The results demonstrate how to design MR-TADF emitters exhibiting both a red-shifting of the emission and a suppression of concentration quenching in the solid state.

2. Results and discussion

2.1 Synthesis

DDiKTa was synthesized in five steps from dimethyl 2,2′-(phenylazanediyl)dibenzoate (Scheme 1). Iodination with *N*-iodosuccinimide (NIS) gave compound **1** in high yield (85%). Saponification followed by acyl chloride formation with $SOCl_2$, and Lewis-acid catalysed Friedel–Crafts acylation afforded key intermediate **2** in 42% yield, the structure of which was confirmed by single crystal X-ray diffraction (Fig. S16, ESI†). Compound **2** was converted to the boronate ester **3** *via* palladium-catalyzed borylation, which was then coupled with a second equivalent of **2** under Suzuki–Miyaura cross-coupling conditions to afford **DDiKTa** in a moderate yield (65%).

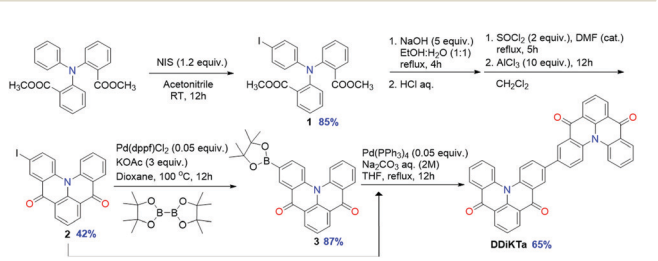

Scheme 1 Synthetic route for **DDiKTa**.

2.2 Computational studies

The frontier molecular orbitals (the HOMO, HOMO−1, LUMO and LUMO+1, see Fig. 1) isocontour plots of **DDiKTa** were obtained based on the optimized ground state gas-phase geometry using Density Functional Theory (DFT) with the PBE0 functional and the 6-31G(d,p) basis set. The calculated dihedral angle between the two **DiKTa** moieties in **DDiKTa** in the ground state is around 37°. The calculated HOMO and LUMO levels of **DDiKTa** are −6.04 and −2.34 eV, respectively. Compared with the reference compound **DiKTa**, the HOMO level of **DDiKTa** is destabilized by 0.16 eV while the LUMO is likewise stabilized by 0.11 eV, both a result of the increased conjugation in **DDiKTa**. The result is a smaller ΔE_{H-L} and an expected red-shift CT absorption compared to **DiKTa** as shown in Fig. S2 (ESI†) according to simulated vertical excitation.

We recently showed the importance of using a suitably high level of theory in order to accurately predict the excited state energies of MR-TADF compounds.[12] Calculations using the Spin-Component Scaling Coupled-Cluster second-order approximate Coupled-Cluster (SCS-CC2) method and the cc-pVDZ level reveal that the short-range charge-transfer character of **DiKTa** (Fig. S2, ESI†) is inherited in **DDiKTa**. The calculated lowest singlet and triplet energy levels of **DDiKTa** are 3.39 and 3.12 eV, respectively, which are slightly lower than those of **DiKTa** (S_1 = 3.45 eV, T_1 = 3.18 eV) and so **DDiKTa** is expected to show a red-shifted emission. As a result, the same ΔE_{ST} of 0.27 eV indicates similar triplet harvesting ability through RISC (see Tables S1 and S2 for a summary of the excited states calculations, ESI†).

2.3 Photophysical properties

The electrochemical behavior of **DDiKTa** was studied by cyclic voltammetry (CV) and differential pulse voltammetry (DPV) in degassed dichloromethane (DCM) with $[n\mathrm{Bu_4N}]PF_6$ as the supporting electrolyte, and the values reported *versus* SCE. The CV and DPV are shown in Fig. 2a and the data for oxidation/reduction potentials (E_{ox}/E_{red}) are summarized in Table S3 (ESI†). **DDiKTa** shows irreversible anodic and reversible cathodic waves. The E_{ox} and E_{red} determined from the DPV peak

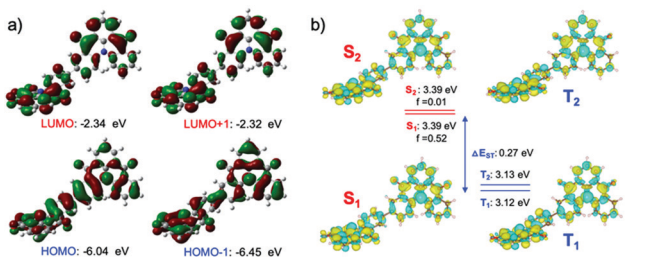

Fig. 1 (a) Isocontour plots (cutoff = 0.02 a.u.) of the HOMO/HOMO−1 and LUMO/LUMO+1 orbitals calculated in the gas phase at the PBE0/6-31G(d,p) level; (b) difference density plots of S_1, S_2, T_1 and T_2 excited states calculated in the gas phase at the SCS-CC2/cc-pVDZ level. *f* indicates the oscillator strength.

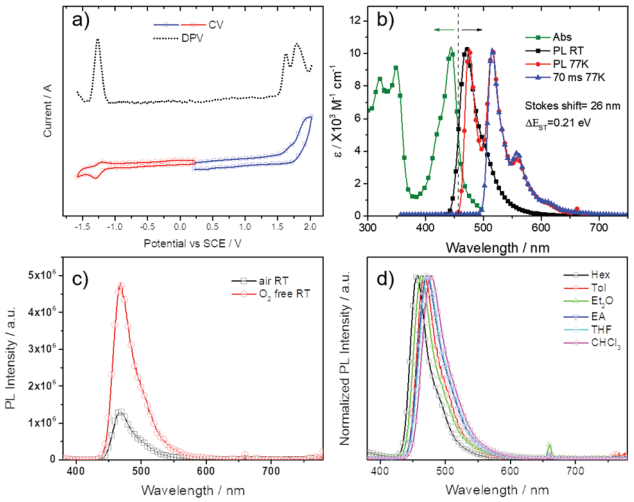

Fig. 2 (a) Cyclic voltammogram (CV) and differential pulse voltammetry (DPV) in degassed DCM with 0.1 M $[n\mathrm{Bu_4N}]\mathrm{PF_6}$ as the supporting electrolyte and $\mathrm{Fc/Fc^+}$ as the internal reference (0.38 V *vs.* SCE). (b) Absorption and steady-state PL spectra obtained in toluene at RT and 77 K, phosphorescence spectra obtained in toluene glass at 77 K (time delay of 70 ms; time window of 140 ms). (c) Comparison of steady-state PL in both aerated and degassed toluene. (d) Solvatochromatic PL study (λ_{exc} = 330 nm).

values are 1.63 and −1.27 V, respectively, showing the expected decreased ΔE due to increased conjugation compared to those of **DiKTa** (E_{ox}: 1.65 eV; E_{red}: −1.33 eV *vs.* SCE; determined from the DPV in MeCN),[21] a trend that is consistent with the DFT calculations. The UV-vis absorption, fluorescence and phosphorescence spectra of **DDiKTa** in dilute toluene solution are depicted in Fig. 2b and the optoelectronic properties are summarized in Table S4 (ESI†). The absorption spectrum exhibits two major absorption bands. The high-energy band from 300–380 nm originates from a π–π* transition of the aromatic skeleton while the broad, low-energy band at 440 nm arises from short-range charge transfer (SRCT) transitions that are characteristic of MR-TADF molecules. Compared to the SRCT absorption band of **DiKTa** at λ_{abs} of 435 nm,[20] that of **DDiKTa** is (i) red-shifted and (ii) broader. The red-shifted emission is supported by SCS-CC2 calculations and the broadened PL spectrum is likely explained by the likely large conformational landscape accessible at room temperature for the torsion between the two **DiKTa** moieties. The room temperature steady-state emission spectrum of **DDiKTa** is similarly red-shifted with λ_{PL} at 470 nm, less structured than **DiKTa** and adversely broadened (FWHM from 27 nm/1251 cm^{-1} for **DiKTa** to 47 nm/1639 cm^{-1} for **DDiKTa**). The mirror image emission spectrum of the absorption spectrum and the small Stokes shift of 26 nm/1291 cm^{-1} suggests a small geometry relaxation in the singlet state (Fig. 2b), highlighting the quite rigid structure of **DDiKTa**. The rigid nature of the compound is also responsible for the narrow emission spectrum observed at RT.

A similar profile but with more pronounced vibronic progression is observed for the phosphorescence spectrum obtained after 70 ms at 77 K in a toluene glass. The ΔE_{ST}, determined from the peak maxima of the fluorescence and

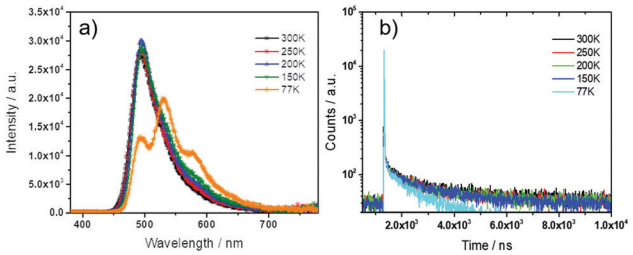

Fig. 3 Temperature-dependent (a) steady-state PL spectra and (b) transient decay characteristics of 9 wt% **DDiKTa** doped into a DPEPO matrix (λ_{exc} = 330 nm).

phosphorescence spectra, of 0.21 eV is sufficiently small to enable a RISC process at room temperature. Fig. 2c shows the oxygen dependency on the intensity of the steady-state PL spectra. The significant drop off in intensity in the emission measured in aerated toluene compared to that after degassing with N_2 clearly demonstrates the contribution from triplet excitons. Similar to **DiKTa** and **Mes3DiKTa**, a modest positive solvatochromism was observed in Fig. 2d in the steady state PL spectra, reflective of the short-range CT state present in MR-TADF emitters.

DPEPO was identified as a suitable host matrix for OLEDs due to its high triplet energy and appropriate HOMO/LUMO levels. The steady-state and transient PL spectra were therefore investigated in 9 wt% doped films of **DDiKTa** in a DPEPO matrix. This concentration was chosen as it corresponds to the doping concentration used in the optimized OLED. As shown in Fig. S5 (ESI†), a similar oxygen dependence on the intensity is also observed, analogous to that seen in toluene. The temperature-dependent steady-state emission of **DDiKTa** in DPEPO is shown in Fig. 3a. The similar intensity of the PL indicates an unexpected temperature independence within the temperature range of 300–150 K, while at 77 K there is a red-shifted and structured emission that is reminiscent of the steady-state emission obtained in toluene glass at 77 K

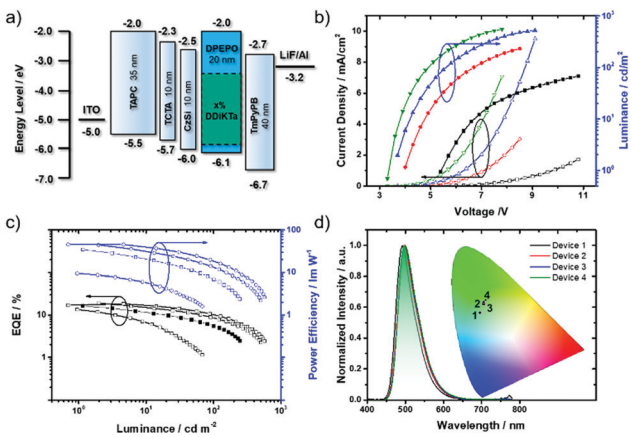

Fig. 4 (a) Device configuration and energy levels for each layer; (b) *J*–*V*–*L* characteristics; (c) EQE and PE *versus* luminance characteristics; (d) electroluminescent spectra for devices with various doping concentrations of **DDiKTa** (inset figure shows the CIE coordinates of four devices).

Table 1 Summary of device performance[a]

Device no.	Doping ratio (%)	λ_{EL}/nm	FWHM/nm	V_{on}[b]/V	CE_{max}/cd A^{-1}	PE_{max}/lm W^{-1}	EQE_{max}/%	CIE(x, y)
Device 1	3	492	55	5.7	23.3	13.5	9.5	0.16, 0.47
Device 2	7	496	58	4.0	44.1	34.6	16.3	0.18, 0.52
Device 3	9	500	59	3.7	52.4	44.4	19.0	0.18, 0.53
Device 4	12	500	59	3.3	52.0	45.4	18.5	0.19, 0.54

[a] The device structure is: ITO/TAPC (35 nm)/TCTA(10 nm)/CzSi(10 nm)/DPEPO: x wt% **DDiKTa**(20 nm)/TmPyPB(40 nm)/LiF(1 nm)/Al. [b] At a luminance of 1 cd m^{-2}.

(Fig. 2b). The steady-state emission at 77 K in DPEPO is a mixture of fluorescence and phosphorescence, which was confirmed by comparing the 77 K prompt fluorescence spectrum integrated by iCDD (time delay after the laser excitation of 0 ns; gate width of 100 ns) and the phosphorescence spectrum integrated by iCDD with a time delay of 1 ms laser excitation and a gate width of 100 ms (Fig. S4b, ESI†). The ΔE_{ST} of 0.16 eV in DPEPO, estimated from the onset of the prompt and phosphorescence spectra, is smaller than that measured in toluene glass (0.21 eV), implying a more efficient RISC process in the former host medium; the activation energy ΔE_a^{TADF} is estimated to be 40 meV (Fig. S6, ESI†). The small activation energy in DPEPO may indicate the involvement of higher-lying excited states in the RISC process. Fig. S4a (ESI†) shows that at room temperature, the prompt emission (time delay of 0 ns; gate width of 10 ns) and the delayed emission (time delay of 1 μs; gate width of 10 μs) align, indicating emission from the S_1 state. The temperature-dependent transient PL (Fig. 3b) reveals a slight decrease of the delayed component with decreasing temperature, indicative of typical TADF behavior.

2.4 Organic light-emitting diodes

To evaluate the potential of **DDiKTa** as an emitter in OLEDs we fabricated several devices, modulating the doping concentration from 3 wt% to 12 wt%, with DPEPO acting as the host matrix. The devices were fabricated with a configuration of: ITO/TAPC (35 nm)/TCTA (10 nm)/CzSi (10 nm)/x wt% **DDiKTa**: DPEPO (20 nm)/TmPyPB (40 nm)/LiF (1 nm)/Al (100 nm) (Fig. 4a), where indium tin oxide (ITO) is the anode, and 4,4′-cyclohexylidenebis[*N*,*N*-bis(4-methylphenyl)benzenamine] (TAPC) and tris(4-carbazoyl-9-ylphenyl)amine (TCTA) act as hole injection and transport layers, respectively. 9-(4-*tert*-Butylphenyl)-3,6-bis(triphenylsilyl)-9*H*-carbazole (CzSi) is used to block excitons and DPEPO is used as the host, 1,3,5-tri(*m*-pyridin-3-ylphenyl)benzene (TmPyPB) acts as the electron-transporting material, and LiF modifies the work function of the aluminum cathode.

Fig. 4b shows the current density–voltage–luminance (J–V–L) characteristics for the four devices. Device 1 with 3 wt% of **DDiKTa** shows a relatively high turn-on voltage at 5.7 V (1 cd m^{-2}), which reveals poor charge injection and mobility in the emitting layer. However, with increasing doping concentration, the turn-on voltage gradually drops to 3.3 V, which can be attributed to the better charge transporting ability of **DDiKTa** than that of DPEPO. Because of the imbalanced charge injection in Device 1, only an EQE_{max} of 9.5% is obtained. Efficiencies can be optimized by increasing the doping concentration over 7 wt%. The best performance obtained at 9 wt%, Device 3, indicates a significant suppression of concentration quenching not normally observed in MR-TADF OLEDs. The EQE_{max} for Devices 3 is 19% with CIE coordinates of (0.18, 0.53), Table 1. Increasing the doping concentration to 12 wt% does not lead to further improvement in performance where the EQE_{max} of Device 4 is 18.5%.

The electroluminescence (EL) spectra for these devices exhibit modest FWHM from 55 to 59 nm that increase with increasing doping concentration. The CIE chromaticity coordinates shift from (0.16, 0.47) for Device 1 to (0.19, 0.54) for Device 4; all OLEDs show green emission (Fig. 4d). In comparison with the EL of **DiKTa**, the red-shifted EL of **DDiKTa** provides a simple design for accessing narrow green MR-TADF OLEDs.

3. Conclusions

In summary, an MR-TADF emitter **DDiKTa** has been developed through a simple dimerization of the previously reported emitter **DiKTa**. This design maintained the multi-resonance TADF photophysical features of its corresponding monomer **DiKTa**. Importantly, the weakly electronically coupled **DiKTa** fragments that result from the twisted confirmation in **DDiKTa** lead to both a red-shifting of the emission and a suppression of concentration quenching, a commonly encountered problem in rigid flat molecules that are emblematic of MR-TADF emitters. The best performing OLED exhibited an EQE_{max} of 19% with an EL maximum of 500 nm. This emitter design indicates the potential to maintain the desirable MR-TADF character of the emitter while extending the conjugation, providing an avenue to MR-TADF emitters in the green and beyond.

Conflicts of interest

There are no conflicts to declare.

Acknowledgements

This project has received funding from the European Union's Horizon 2020 research and innovation programme under the Marie Skłodowska Curie grant agreement No. 838009 (TSFP) and No. 838885 (NarrowbandSSL). D. S. acknowledges support from the Marie Skłodowska-Curie Individual Fellowship, the National Postdoctoral Program for Innovative Talents (BX201700164), and the Jiangsu Planned Projects for Postdoctoral Research Funds (2018K011A). The St Andrews team would also like to thank the

Leverhulme Trust (RPG-2016047) and EPSRC (EP/P010482/1) for financial support. We thank Umicore AG for the gift of materials. Computational resources have been provided by the Consortium des Équipements de Calcul In-tensif (CÉCI), funded by the Fonds de la Recherche Scientifiques de Belgique (F. R. S.-FNRS) under Grant no. 2.5020.11. YO acknowledge fruitful discussion with Prof. D. Beljonne from the University of Mons, Prof. Juan-Carlos Sancho-Garcia from the University of Alicante and Prof. L. Muccioli from the University of Bologna.

Notes and references

1 Y. Tao, K. Yuan, T. Chen, P. Xu, H. Li, R. Chen, C. Zheng, L. Zhang and W. Huang, Thermally Activated Delayed Fluorescence Materials Towards the Breakthrough of Organoelectronics, *Adv. Mater.*, 2014, **26**(47), 7931–7958.

2 M. Y. Wong and E. Zysman-Colman, Purely Organic Thermally Activated Delayed Fluorescence Materials for Organic Light-Emitting Diodes, *Adv. Mater.*, 2017, **29**(22), 1605444.

3 Y. Liu, C. Li, Z. Ren, S. Yan and M. R. Bryce, All-organic thermally activated delayed fluorescence materials for organic light-emitting diodes, *Nat. Rev. Mater.*, 2018, **3**(4), 18020.

4 Y. Olivier, J. C. Sancho-Garcia, L. Muccioli, G. D'Avino and D. Beljonne, Computational Design of Thermally Activated Delayed Fluorescence Materials: The Challenges Ahead, *J. Phys. Chem. Lett.*, 2018, **9**(20), 6149–6163.

5 X. Liang, Z.-L. Tu and Y.-X. Zheng, Thermally Activated Delayed Fluorescence Materials: Towards Realization of High Efficiency Through Strategic Small Molecular Design, *Chem. – Eur. J.*, 2019, **25**(22), 5623–5642.

6 Y. Im, M. Kim, Y. J. Cho, J.-A. Seo, K. S. Yook and J. Y. Lee, Molecular Design Strategy of Organic Thermally Activated Delayed Fluorescence Emitters, *Chem. Mater.*, 2017, **29**(5), 1946–1963.

7 Y. J. Cho, S. K. Jeon, S.-S. Lee, E. Yu and J. Y. Lee, Donor Interlocked Molecular Design for Fluorescence-like Narrow Emission in Deep Blue Thermally Activated Delayed Fluorescent Emitters, *Chem. Mater.*, 2016, **28**(15), 5400–5405.

8 I. S. Park, K. Matsuo, N. Aizawa and T. Yasuda, High-Performance Dibenzoheteraborin-Based Thermally Activated Delayed Fluorescence Emitters: Molecular Architectonics for Concurrently Achieving Narrowband Emission and Efficient Triplet–Singlet Spin Conversion, *Adv. Funct. Mater.*, 2018, **28**(34), 1802031.

9 Y. Im, S. H. Han and J. Y. Lee, Deep blue thermally activated delayed fluorescent emitters using CN-modified indolocarbazole as an acceptor and carbazole-derived donors, *J. Mater. Chem. C*, 2018, **6**(18), 5012–5017.

10 D. H. Ahn, S. W. Kim, H. Lee, I. J. Ko, D. Karthik, J. Y. Lee and J. H. Kwon, Highly efficient blue thermally activated delayed fluorescence emitters based on symmetrical and rigid oxygen-bridged boron acceptors, *Nat. Photonics*, 2019, **13**(8), 540–546.

11 P. Rajamalli, N. Senthilkumar, P. Y. Huang, C. C. Ren-Wu, H. W. Lin and C. H. Cheng, New Molecular Design Concurrently Providing Superior Pure Blue, Thermally Activated Delayed Fluorescence and Optical Out-Coupling Efficiencies, *J. Am. Chem. Soc.*, 2017, **139**(32), 10948–10951.

12 A. Pershin, D. Hall, V. Lemaur, J.-C. Sancho-Garcia, L. Muccioli, E. Zysman-Colman, D. Beljonne and Y. Olivier, Highly emissive excitons with reduced exchange energy in thermally activated delayed fluorescent molecules, *Nat. Commun.*, 2019, **10**(1), 597.

13 J. P. Spindler, T. K. Hatwar, M. E. Miller, A. D. Arnold, M. J. Murdoch, P. J. Kane, J. E. Ludwicki, P. J. Alessi and S. A. Van Slyke, System considerations for RGBW OLED displays, *J. Soc. Inf. Disp.*, 2006, **14**(1), 37–48.

14 H. Hirai, K. Nakajima, S. Nakatsuka, K. Shiren, J. Ni, S. Nomura, T. Ikuta and T. Hatakeyama, One-Step Borylation of 1, 3-Diaryloxybenzenes Towards Efficient Materials for Organic Light-Emitting Diodes, *Angew. Chem., Int. Ed.*, 2015, **54**(46), 13581–13585.

15 T. Hatakeyama, K. Shiren, K. Nakajima, S. Nomura, S. Nakatsuka, K. Kinoshita, J. Ni, Y. Ono and T. Ikuta, Ultrapure blue thermally activated delayed fluorescence molecules: efficient HOMO–LUMO separation by the multiple resonance effect, *Adv. Mater.*, 2016, **28**(14), 2777–2781.

16 S. H. Han, J. H. Jeong, J. W. Yoo and J. Y. Lee, Ideal blue thermally activated delayed fluorescence emission assisted by a thermally activated delayed fluorescence assistant dopant through a fast reverse intersystem crossing mediated cascade energy transfer process, *J. Mater. Chem. C*, 2019, **7**(10), 3082–3089.

17 X. Liang, Z.-P. Yan, H.-B. Han, Z.-G. Wu, Y.-X. Zheng, H. Meng, J.-L. Zuo and W. Huang, Peripheral amplification of multi-resonance induced thermally activated delayed fluorescence for highly efficient OLEDs, *Angew. Chem., Int. Ed.*, 2018, **130**(35), 11486–11490.

18 Y. Kondo, K. Yoshiura, S. Kitera, H. Nishi, S. Oda, H. Gotoh, Y. Sasada, M. Yanai and T. Hatakeyama, Narrowband deep-blue organic light-emitting diode featuring an organoboron-based emitter, *Nat. Photonics*, 2019, **13**(10), 678–682.

19 X. Li, Y. Shi, K. Wang, M. Zhang, C.-J. Zheng, D.-M. Sun, G. Dai, X.-C. Fan, D.-Q. Wang and W. Liu, Thermally Activated Delayed Fluorescence Carbonyl Derivatives for Organic Light Emitting Diodes with Extremely Narrow Full-Width at Half-Maximum, *ACS Appl. Mater. Interfaces*, 2019, **11**(14), 13472–13480.

20 Y. Yuan, X. Tang, X. Y. Du, Y. Hu, Y. J. Yu, Z. Q. Jiang, L. S. Liao and S. T. Lee, The Design of Fused Amine/Carbonyl System for Efficient Thermally Activated Delayed Fluorescence: Novel Multiple Resonance Core and Electron Acceptor, *Adv. Opt. Mater.*, 2019, **7**(7), 1801536.

21 D. Hall, S. M. Suresh, P. L. dos Santos, E. Duda, S. Bagnich, A. Pershin, P. Rajamalli, D. B. Cordes, A. M. Slawin and D. Beljonne, Improving Processability and Efficiency of Resonant TADF Emitters: A Design Strategy, *Adv. Opt. Mater.*, 2020, **8**(2), 1901627.

22 Y. Zhang, D. Zhang, J. Wei, Z. Liu, Y. Lu and L. Duan, Multi-Resonance Induced Thermally Activated Delayed Fluorophores for Narrowband Green OLEDs, *Angew. Chem., Int. Ed.*, 2019, **131**(47), 17068–17073.

